



A Journal of the Gesellschaft Deutscher Chemiker

Angewandte Chemie

GDCh

International Edition

www.angewandte.org

Accepted Article

Title: Photochemical in-situ Exfoliation of Metal–Organic Frameworks for Enhanced Visible-Light-Driven CO₂ Reduction

Authors: Hui-Li Zheng, Shan-Lin Huang, Ming-Bu Luo, Qin Wei, Er-Xia Chen, Liang He, and Qipu Lin

This manuscript has been accepted after peer review and appears as an Accepted Article online prior to editing, proofing, and formal publication of the final Version of Record (VoR). This work is currently citable by using the Digital Object Identifier (DOI) given below. The VoR will be published online in Early View as soon as possible and may be different to this Accepted Article as a result of editing. Readers should obtain the VoR from the journal website shown below when it is published to ensure accuracy of information. The authors are responsible for the content of this Accepted Article.

To be cited as: *Angew. Chem. Int. Ed.* 10.1002/anie.202012019

Link to VoR: <https://doi.org/10.1002/anie.202012019>

Photochemical *in-situ* Exfoliation of Metal–Organic Frameworks for Enhanced Visible-Light-Driven CO₂ Reduction

Hui-Li Zheng,^[a] Shan-Lin Huang,^[a] Ming-Bu Luo,^[a] Qin Wei,^[a] Er-Xia Chen,^[a] Liang He,^[a] Qipu Lin*^[a]

[a] H.-L. Zheng, S.-L. Huang, M.-B. Luo, Q. Wei, E.-X. Chen, L. He, Prof. Q. Lin
State Key Laboratory of Structural Chemistry,
Fujian Institute of Research on the Structure of Matter,
Chinese Academy of Sciences, Fuzhou, 350002, China.
E-mail: linqipu@fjirsm.ac.cn

Supporting information for this article can be found under: <http://dx.doi.org/10.1002/anie.x0xx00000x>.

Abstract: Two novel two-dimensional metal–organic frameworks (2D MOF), 2D-M₂TCPE (M = Co or Ni, TCPE = 1,1,2,2-tetra(4-carboxyphenyl)ethylene), which are composed of staggered (4,4)-grid layers based on paddlewheel-shaped dimers, serve as heterogeneous photocatalysts and achieve efficient reduction of CO₂ to CO. During the visible-light-driven catalysis, these structures undergo *in-situ* exfoliation to form nanosheets, which exhibit excellent stability and improved catalytic activity. The exfoliated 2D-M₂TCPE nanosheets display a high CO evolution rate of 4174 μmol g⁻¹ h⁻¹ and high selectivity of 97.3% for M = Co and Ni, and thus they are superior to most reported MOFs. The performance differences and photocatalytic mechanisms have been studied with theoretical calculations and photoelectric experiments. This work proposes a new insight for the controllable synthesis of effective crystalline photocatalysts based on structural and morphological co-regulation.

Because of the excessive use of carbon fossil fuels, the greenhouse effect and the energy crisis are becoming increasingly severe and could threaten the human survival in the future. Advanced methods and technologies to reduce CO₂ emissions and achieve energy regeneration are much sought after.^[1,2] Photocatalytic reduction of CO₂ leading ultimately to added-value chemicals is one of the best ways to solve these issues, because it promises both greenhouse gas elimination and an alternative means of energy production.^[3,4] However, due to the poor reactivity of CO₂ and a process involving multi-electron transfer, the activation and reduction of CO₂ is challenging and requires an efficient catalyst.^[5] Recently, many catalysts for CO₂ reduction have been extensively studied, but the application is still hampered by low efficiency, poor selectivity, instability and an unclear mechanism.^[6] Consequently, new material systems and rational design of highly efficient photocatalysts remain crucial and challenging.

Metal–organic frameworks (MOF) as an emerging class of porous materials with precise structures have unique advantages for photocatalytic reactions including their controllable structure, high surface area, excellent ability to capture CO₂ and their photochemical characteristics.^[7,8] By selecting preset organic ligands and metal cations or clusters, open active sites which can stabilize the reaction intermediates and depress the energy barrier to adsorb and activate CO₂ molecules can be constructed.^[9,10] Most of the MOFs currently reported to be involved in the photocatalytic reduction of CO₂ however exist in the form of solid blocks, which inevitably affects the expression of their catalytic activity due to limitations in their morphology and thickness.^[11] Compared with such bulk materials, MOFs with a 2D conformation have an increased surface area which enhances the contact between the catalyst

surface and CO₂ molecules, and can minimize the pathways associated with electron transport.^[12] It is possible to improve the photocatalytic performance of layered MOFs by exfoliation, a process in which the bulk phases are converted into ultrathin 2D nanosheets. To date, due to the difficulty of mechanical exfoliation or direct synthesis of nanosheets, there are only a few reports of the use of 2D MOFs for photocatalytic reduction of CO₂, and there is an urgent need for methods by which they can be prepared.^[13] Photochemical exfoliation has a powerful potential as an effective method for achieving ultrathin materials, because it can expose more active sites and improve the microenvironment of the catalyst-solution interface to enhance catalytic activity.^[14] Therefore, promotion of the spontaneous conversion of bulk MOFs into 2D nanosheets by photocatalytic *in-situ* exfoliation is a promising strategy.

Continuing our previous work on the photoreduction of CO₂,^[15] we designed and synthesized two new 2D MOFs, [Ni₂(TCPE)(H₂O)₄]_n (2D-Ni₂TCPE) and [Co₂(TCPE)(H₂O)₄]_n (2D-Co₂TCPE), which are based on the tetracarboxylate-bridged paddlewheel-shaped dimeric secondary building units (SBU), and could have a large number of open metal sites once removal of the axially-coordinated water is achieved. The resulting staggered, weakly interacting layer structure could induce the bulk 2D MOFs to realize *in-situ* exfoliation under the photochemical conditions. As the photocatalytic CO₂ reaction progresses, the bulk material is gradually stripped into nanosheets and presents a Tyndall effect, with which the exfoliated nanosheets can efficiently reduce CO₂ under visible light irradiation giving a high CO evolution rate (4174 μmol g⁻¹ h⁻¹) and high selectivity (97.3%) for 2D-Co₂TCPE and 2D-Ni₂TCPE, respectively. To the best of our knowledge, this is the first time the formation of 2D MOF nanosheets using photochemical exfoliation *in-situ* to enhance the photocatalytic reduction of CO₂. We examined the mechanism of the catalysis in detail through density functional theory (DFT) calculations and experiments based on clear structural information about MOFs. Our results have provided a model and a basis for further discussion of structure-activity relationships of MOF-based materials in CO₂ reduction.

Single crystal X-ray diffraction (SCXRD) analysis revealed that 2D-Ni₂TCPE and 2D-Co₂TCPE both crystallize in an orthorhombic space group P222₁ (Table S1). As shown in Figure 1a, these 2D MOFs are isostructural, and consist of paddlewheel-like SBUs of [M₂(COO)₄(H₂O)₂] (M = Ni, Co) formed by two independent metal atoms, four carboxyl groups and two axially-coordinated water molecules. Each TCPE spacer connects four SBUs and a 2D (4,4)-grid layer with rhomboid windows is built from these moieties (Figure 1b).

Adjacent layers are staggered in an ABAB manner (Figure 1c), which is probably beneficial to exfoliation. In addition, the weakly-coordinated axial H₂O is easily removed, leaving open metal sites (OMS) which facilitate the adsorption and activation of CO₂.^[16] Co/Ni-based 2D MOFs based on paddlewheel-shaped SBUs with OMSs are uncommon (Figure S1). Powder X-ray diffraction patterns (PXRD) confirm the phase purity of 2D-Ni₂TCPE and 2D-Co₂TCPE (Figure S2) and their thermal stability was characterized by thermogravimetric analysis (TGA) (Figure S3). The CO₂ uptake values of 2D-Ni₂TCPE and 2D-Co₂TCPE at 273 K were determined to be 36.5 and 41.7 cm³ g⁻¹, respectively, suggesting their potential for CO₂ adsorption (Figure S4).^[17]

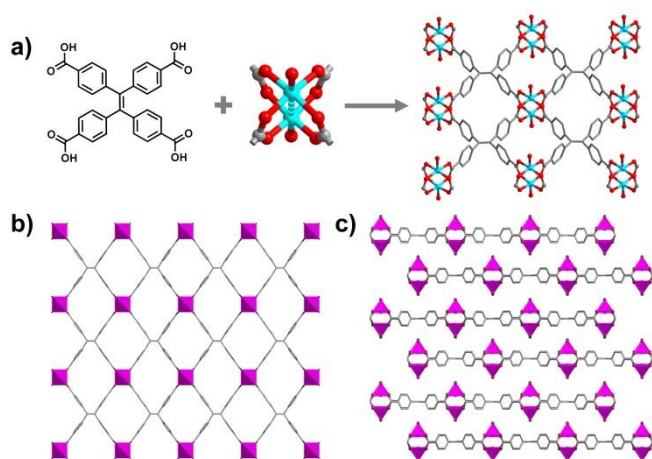


Figure 1. a) The single-crystal structure of 2D-M₂TCPE (M = Ni, Co) based on a TCPE linker and a paddlewheel-like node; b, c) The (4,4)-grid monolayer, and its staggered arrangement in an ABAB manner.

The UV-Vis absorption spectra of these 2D MOFs reveals a broad absorption in the region of 450–800 nm, which indicates their potential for photocatalytic reactions (Figure S5). According to the Tauc plot, band gap energies (E_g) of 2.63 and 2.70 eV were obtained for 2D-Ni₂TCPE and 2D-Co₂TCPE, respectively (Figure S6). Mott-Schottky measurements revealed the intrinsic characteristics of an n-type semiconductor, and the flat potential of 2D-Ni₂TCPE and 2D-Co₂TCPE vs. Ag/AgCl was determined to be -1.12 and -1.20 eV, respectively (Figure S7). Therefore, the positions of conduction bands (CB) were determined to be -0.92 and -1.10 eV vs. NHE for 2D-Ni₂TCPE and 2D-Co₂TCPE, respectively.^[18] Their positions of CB are more negative than the reduction potential of CO₂ to CO (-0.51 eV vs. NHE, pH = 7), which indicates that a photoexcited electron can be transferred from the catalyst 2D-M₂TCPE to the CO₂ molecules adsorbed on OMSs of SBUs.

The photocatalytic activity of 2D-Ni₂TCPE and 2D-Co₂TCPE was evaluated by visible-light driven CO₂ reduction reactions conducted in a CO₂-saturated CH₃CN/H₂O mixed solvent system with [Ru(bpy)₃]Cl₂·6H₂O (bpy = 2,2'-bipyridine) as the photosensitizer and triethanolamine (TEOA) as an electron donor. As shown in Figure 2a, the amount of CO produced gradually increases with illumination time until the rate of increase tends to be steady at ~10 h with a maximum yield of 100 μmol. Compared with CO, the amount of H₂ formed from H₂O also increases with illumination time accompanied by a

negligible increase in the rate of the reaction. During the whole photocatalytic reaction of 2D-Ni₂TCPE, the average CO evolution rate reaches 2000 μmol g⁻¹ h⁻¹ with a high selectivity of 97.2% over the competing H₂ generation. In contrast, 2D-Co₂TCPE displays a higher CO evolution rate of 2560 μmol g⁻¹ h⁻¹ and H₂ evolution rates of 200 μmol g⁻¹ h⁻¹ with the selectivity of CO only 75.8% (Figures 2b and S8). The liquid phase product was detected by ¹H nuclear magnetic resonance (NMR), and no formic acid or methanol was observed, indicating that CO is the only CO₂ reduction product (Figure S9). The conditions for CO production were analyzed in a series of comparative experiments and the results show that significant reduction products were detected only in the presence of 2D-M₂TCPE, a photosensitizer, TEOA and light (Figure S10, Table S4). In order to verify the source of CO, we replaced CO₂ with N₂ and conducted experiments under the same conditions. As a result, after 10 h of visible light irradiation, only traces of CO were detected, indicating that the previously observed CO was indeed derived from CO₂. When the isotopically-labeled ¹³CO₂ replaced CO₂ in the photocatalytic experiments and the generated ¹³CO was analyzed by gas chromatography-mass spectrometry (GC-MS), the peak with $m/z = 29$ corresponded to ¹³CO, further proving that the source of CO is CO₂ rather than the decomposition of other organic components in the reaction system (Figures 2c and S11).

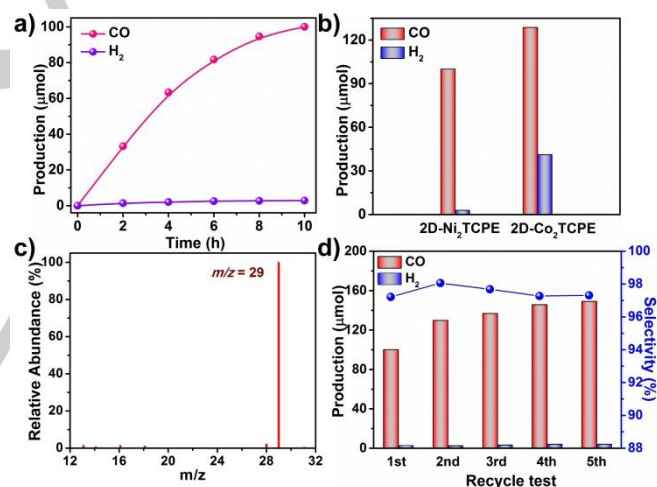


Figure 2. a) The photocatalytic production of CO and H₂ as a function of reaction time over 2D-Ni₂TCPE; b) The comparison of amount of CO and H₂ produced by 2D-Ni₂TCPE and 2D-Co₂TCPE; c) The mass spectral analysis of the produced ¹³CO; d) The recycling examination of 2D-Ni₂TCPE with 10 h of each run.

In order to examine the photocatalytic stability of 2D-Ni₂TCPE, we recycled the catalyzed sample for five runs with the same reaction conditions. As shown in Figures 2d and S12, it was found that the yield amount of CO was not reduced but rather increased with the cycle number. In the 5th run with 2D-Ni₂TCPE, the amount of CO was 110 μmol and the evolution rate was 3000 μmol g⁻¹ h⁻¹ maintaining a relatively stable selectivity of 97.3%. The same result was obtained from the cyclic testing of 2D-Co₂TCPE, and the increase ratio here was particularly prominent, promoting an increase in the CO evolution rate to 4174 μmol g⁻¹ h⁻¹ in the 5th run (Figure S13).

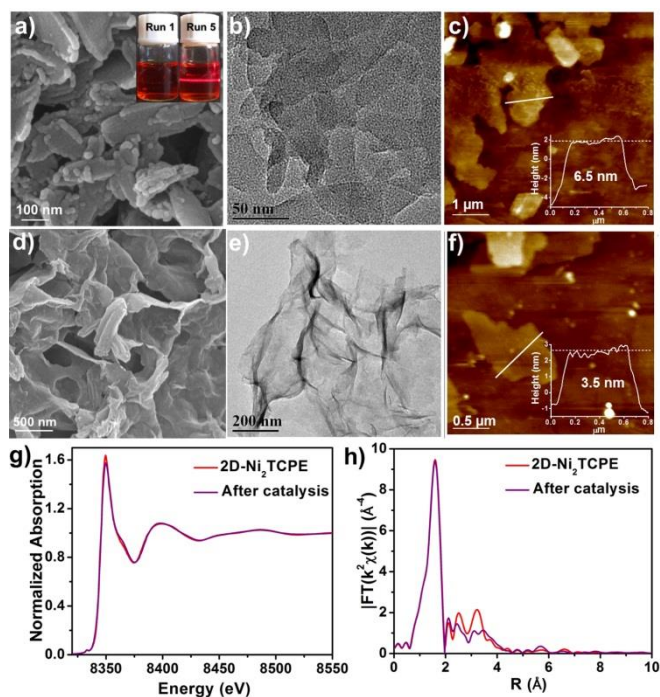


Figure 3. The SEM, TEM and AFM images for 2D-Ni₂TCPE-PE (a-c) and 2D-Ni₂TCPE-ME (d-f); g-h) EXAFS and XANES of 2D-Ni₂TCPE before and after the photocatalytic CO₂ reduction. Inset of a): A photograph of the Tyndall effect of the solution after the 1st and 5th run.

As the cycling experiment progressed, the Tyndall effect of the solution after each run was clearly enhanced. This showed that the size of 2D-Ni₂TCPE particles is gradually reduced towards that of nanocrystals (Figure S14). In view of their structural features, these 2D MOF materials may be stripped into nanosheets to activate their powerful catalytic potential during the catalytic reaction process. The scanning electron microscopy (SEM) and transmission electron microscopy (TEM) images clearly reveal that the 2D-Ni₂TCPE was exfoliated from the original bulk material into uniform nanosheets of 2D-Ni₂TCPE-PE (PE = photochemical exfoliation, Figures 3a-3b and S15). An atomic force microscopy (AFM) image demonstrates the nanosheet structure of resultant 2D-Ni₂TCPE-PE, whose average thickness is approximately 6.5 nm (Figure 3c). Together, the above characterizations show that the ultrathin nanosheet of 2D-Ni₂TCPE was successfully obtained by *in-situ* exfoliation during the photochemical CO₂ reduction. To further verify experimentally that the enhanced activity comes from the change in the nanotopography, 2D-Ni₂TCPE-ME (ME = mechanical exfoliation) was prepared by manual mechanical exfoliation (see Supporting Information for details) and applied to photocatalytic CO₂ reduction under the same experimental conditions (Figures 3d-3e and S16). As shown in Figure 3f, the mechanically exfoliated 2D-Ni₂TCPE-ME also exhibits a very uniform nanosheet structure with a thickness of approximately 3.5 nm, and its average CO evolution rate of 2D-Ni₂TCPE-ME reaches 2940 μmol g⁻¹ h⁻¹ with a high selectivity of 96.9 %, and thus has an absolute advantage over bulk materials (Figure S17). Accordingly, the overall performance of 2D-M₂TCPE nanosheets is much higher than most MOFs reported as heterogeneous photocatalysts under similar operation conditions (Tables S5 and S6). Compared with crystalline bulk materials,

the nanosheet 2D-Ni₂TCPE can increase the exposed surfaces, shorten the route of electron transport and facilitate the separation and transport of photogenerated carriers to enhance the cooperative photocatalytic activity.^[5a,13,19] Benefiting from the similar structural features of 2D-Ni₂TCPE, few-layered 2D-Co₂TCPE can also be obtained by photochemical *in-situ* exfoliation and can achieve its nanosized thickness by controlling the cycle number (Figure S18). PXRD after cycling testing demonstrates that the recycled samples have crystallinity and maintain the main peak positions of the original sample (Figure S19). To further confirm the local coordination environment of the metal atom and the structural stability after the reaction, the Ni and Co K-edge extended X-ray absorption fine structure (EXAFS) and X-ray absorption near-edge structure (XANES) spectroscopies were examined (Figures 3g-3h, S20). The valence states and coordination environments of Ni or Co in these MOFs before and after catalysis are essentially unchanged, which indicates their excellent stability. Additionally, characterization after reaction by high resolution transmission electron microscopy (HR-TEM), Fourier transform-infrared spectroscopy (FT-IR) and X-ray photoelectron spectroscopy (XPS) confirmed that 2D-Ni₂TCPE and 2D-Co₂TCPE are structurally stable (Figures S21-S24).

To further study the process of photogenerated electron transfer between photosensitizer and catalyst, photoluminescent (PL) quenching experiments were performed on a solution in CH₃CN/H₂O of [Ru(bpy)₃]Cl₂ with a catalyst or an electron sacrificial agent, TEOA. As shown in Figure 4a, the PL intensity of [Ru(bpy)₃]Cl₂ gradually decreases with the increase of the amount of the catalyst 2D-Ni₂TCPE, suggesting that the photo-generated electrons can be transferred from the excited state of [Ru(bpy)₃]Cl₂ to 2D-Ni₂TCPE.^[20] In contrast, the PL intensity is not quenched significantly by increasing the amount of TEOA, which shows that the excited state of [Ru(bpy)₃]Cl₂ can be oxidative and is quenched by the catalyst 2D-Ni₂TCPE in the photocatalytic system (Figure S25).^[21] In addition, the lifetime of [Ru(bpy)₃]Cl₂ solution was characterized by the steady-state and time-resolved emission spectroscopy and fitted to be 565 ns (Figure 4b). The lifetime significantly diminishes upon addition of the catalyst 2D-Ni₂TCPE to [Ru(bpy)₃]Cl₂ solution, and was determined to reach 352 ns. This shortened PL lifetime indicates that photogenerated electrons can be rapidly transferred from [Ru(bpy)₃]Cl₂ to the catalyst 2D-Ni₂TCPE, effectively inhibiting the recombination of photogenerated carriers.^[22] Compared with 2D-Ni₂TCPE, the catalyst 2D-Co₂TCPE shows a more obvious PL quenching effect and a correspondingly shorter lifetime decay of 332 ns at the same equivalent catalyst loading (Figure S26). These observations indicate that 2D-Co₂TCPE is better able to inhibit the recombination of photogenerated electrons and holes and consequently exhibits higher photocatalytic activity.^[23] The photoelectrochemical measurements show that both catalysts possessed rapid photocurrent responses and good reproducibility under visible light irradiation over several minutes (Figure S27). 2D-Co₂TCPE is significantly more effective than 2D-Ni₂TCPE at separating photogenerated electron-hole pairs under the same conditions, further showing that the former has a higher catalytic activity.

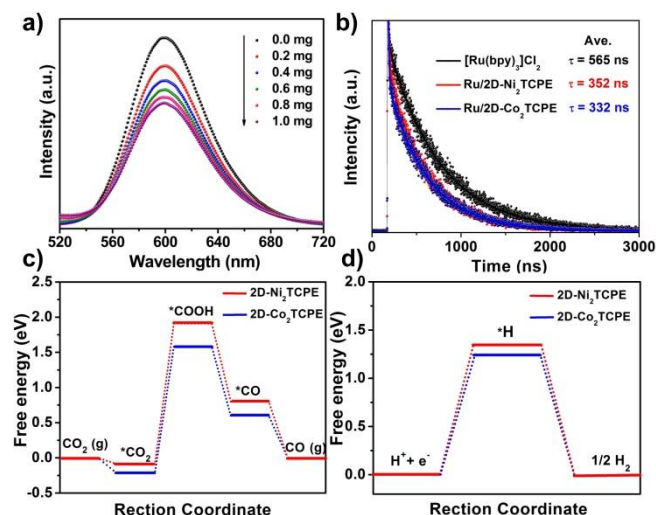


Figure 4. a) The steady state fluorescence spectra of [Ru(bpy)₃]Cl₂ upon the addition of 2D-Ni₂TCPE ($\lambda_{\text{ex}} = 375$ nm); b) The time-resolved fluorescence decay spectra of [Ru(bpy)₃]Cl₂ (Ru) with and without 2D-Ni₂TCPE or 2D-Co₂TCPE; c) The calculated free energy profile of photocatalytic CO₂ reduction toward CO; d) The calculated free energy diagram of photocatalytic H₂ production.

DFT calculations were performed to further explore the differences in catalytic activity between 2D-Ni₂TCPE and 2D-Co₂TCPE. The adsorption energy of CO₂ on 2D-Co₂TCPE is stronger than that on 2D-Ni₂TCPE (Table S7), suggesting the stronger adsorption affinity of 2D-Co₂TCPE for CO₂, a finding which is also supported by CO₂ isotherm measurements. In order to gain insight into the CO₂ reduction process, DFT calculations were used to investigate the energetics of CO₂ reduction (Figure S28). Previous studies have shown that formation of *COOH is the rate-determining step for reduction of CO₂ to CO.^[20a,24] Thus, an efficient CO₂ reduction catalyst would be expected to favor the *COOH formation. The results shown in Figure 4c, reveal that the potential energy barriers of 2D-Co₂TCPE and 2D-Ni₂TCPE reducing *CO₂ to *COOH are 1.80 and 2.00 eV, respectively, which confirms that 2D-Co₂TCPE has greater thermodynamic potential for CO₂ reduction. In addition, the free energy of photocatalytic hydrogen evolution reaction (HER) was calculated as 1.24 eV for 2D-Co₂TCPE and 1.34 eV for 2D-Ni₂TCPE (Figure 4d, S29). These results imply that 2D-Ni₂TCPE shows better selectivity than 2D-Co₂TCPE due to its higher HER free energy, and this matches the experimental results. From the results of these experiments and theoretical calculations, we proposed a possible mechanism of photocatalytic reduction of CO₂ (Figure S30). Under the excitation of visible light, the photosensitizer [Ru(bpy)₃]²⁺ is excited and forms [Ru(bpy)₃]^{2+*}, which is then reductively quenched by the TEOA to generate the reduced species, i.e. [Ru(bpy)₃]⁺. Since the LUMO value of 2D-M₂TCPE is lower than that of [Ru(bpy)₃]²⁺, the photo-generated electrons can be transferred from the LUMO of [Ru(bpy)₃]²⁺ to the surface of 2D-M₂TCPE (Figure S31). The transferred electrons are accepted by the CO₂ adsorbed on the open metal sites of the catalyst to form the *CO₂⁻ intermediate. This is the pivotal step of the reaction, after which the *CO₂⁻ is finally reduced to CO with the participation of a proton.

In summary, we have developed a controllable and simple multilevel regulation strategy for photocatalytic CO₂ reduction based on rational structural design and structure-directed morphology control to improve its efficiency. Well-constructed paddlewheel-shaped units with weakly coordinated water molecules in 2D MOFs show unique advantages by exposing more active sites to promote CO₂ adsorption and catalytic conversion. Furthermore, the weak van der Waals effect between staggered layers of MOFs is favorable for *in-situ* exfoliation to form nanosheets under photochemical stimuli. These nanosheets shorten the path of electron transport and facilitate the separation and transport of photogenerated carriers to enhance the cooperative photocatalytic activity. Based on such dual regulation, these layered MOFs display excellent catalytic activity and high selectivity, and are therefore preferable to most previously reported MOF-based catalysts. This work not only presents a rare example of photochemically-driven *in-situ* exfoliation to enhance CO₂ photoreduction, but also opens a promising approach to preparation of 2D nanomaterials and efficient photocatalysts through a design developed at the molecular level.

Acknowledgements

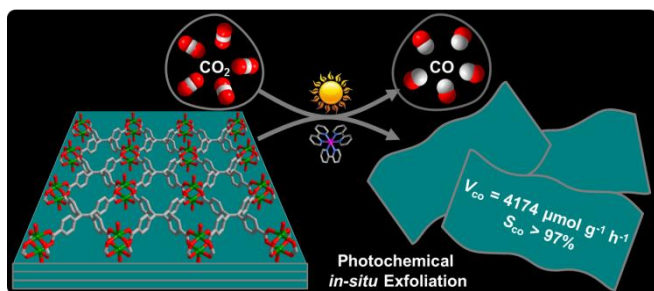
This work was supported by the Strategic Priority Research Program of Chinese Academy of Sciences (Grant No. XDB20000000) and the Hundred-Talent Program of Fujian Province.

Keywords: 2D metal–organic frameworks • *in-situ* exfoliation • nanosheets • photocatalytic CO₂ reduction

- [1] a) M. Ding, R. W. Flaig, H.-L. Jiang, O. M. Yaghi, *Chem. Soc. Rev.* **2019**, *48*, 2783-2828; b) M. Aresta, A. Dibenedetto, A. Angelini, *Chem. Rev.* **2014**, *114*, 1709-1742.
- [2] a) Y.-S. Wei, M. Zhang, R. Zou, Q. Xu, *Chem. Rev.* **2020**, 10.1021/acs.chemrev.9b00757; b) Y.-N. Gong, L. Jiao, Y. Qian, C.-Y. Pan, L. Zheng, X. Cai, B. Liu, S.-H. Yu, H.-L. Jiang, *Angew. Chem., Int. Ed.* **2020**, *59*, 2705-2709; c) J. Han, P. An, S. Liu, X. Zhang, D. Wang, Y. Yuan, J. Guo, X. Qiu, K. Hou, L. Shi, Y. Zhang, S. Zhao, C. Long, Z. Tang, *Angew. Chem., Int. Ed.* **2019**, *58*, 12711-12716.
- [3] a) X. Li, Y. Sun, J. Xu, Y. Shao, J. Wu, X. Xu, Y. Pan, H. Ju, J. Zhu, Y. Xie, *Nat. Energy* **2019**, *4*, 690-699; b) J. L. White, M. F. Baruch, J. E. Pander, Y. Hu, I. C. Fortmeyer, J. E. Park, T. Zhang, K. Liao, J. Gu, Y. Yan, T. W. Shaw, E. Abelev, A. B. Bocarsly, *Chem. Rev.* **2015**, *115*, 12888-12935.
- [4] a) N.-N. Vu, S. Kaliaguine, T.-O. Do, *Adv. Funct. Mater.* **2019**, *29*, 1901825-1901868; b) A. Dhakshinamoorthy, A. M. Asiri, H. Garcia, *Adv. Mater.* **2019**, *31*, 1900617-1900656; c) C. Gao, Q. Meng, K. Zhao, H. Yin, D. Wang, J. Guo, S. Zhao, L. Chang, M. He, Q. Li, H. Zhao, X. Huang, Y. Gao, Z. Tang, *Adv. Mater.* **2016**, *28*, 6485-6490; d) M. Wang, D. Wang, Z. Li, *Appl. Catal. B: Environ.* **2016**, *183*, 47-52.
- [5] a) Y. Wang, S. Wang, S. L. Zhang, X. W. Lou, *Angew. Chem., Int. Ed.* **2020**, *59*, 11918-11922; b) A. Dhakshinamoorthy, Z. Li, H. Garcia, *Chem. Soc. Rev.* **2018**, *47*, 8134-8172; c) K. Maeda, *Adv. Mater.* **2019**, *31*, 1808205.
- [6] a) X. Jiao, K. Zheng, L. Liang, X. Li, Y. Sun, Y. Xie, *Chem. Soc. Rev.* **2020**, 10.1039/D0CS00332H; b) J. Ran, M. Jaroniec, S.-Z. Qiao, *Adv. Mater.* **2018**, *30*, 1704649.
- [7] a) J.-D. Xiao, H.-L. Jiang, *Acc. Chem. Res.* **2019**, *52*, 356-366; b) Y. Wang, N.-Y. Huang, J.-Q. Shen, P.-Q. Liao, X.-M. Chen, J.-P. Zhang, *J. Am. Chem. Soc.* **2018**, *140*, 38-41; c) J. Lu, N. S. Khatri, J. A.

- Johnson, X. C. Zeng, J. Zhang, *J. Am. Chem. Soc.* **2016**, *138*, 15805-15808.
- [8] a) J. Dong, X. Han, Y. Liu, H. Li, Y. Cui, *Angew. Chem., Int. Ed.* **2020**, *59*, 13722-13733; b) Y.-H. Luo, L.-Z. Dong, J. Liu, S.-L. Li, Y.-Q. Lan, *Coord. Chem. Rev.* **2019**, *390*, 86-126; c) Z.-B. Fang, T.-T. Liu, J. Liu, S. Jin, X.-P. Wu, X.-Q. Gong, K. Wang, Q. Yin, T.-F. Liu, R. Cao, H.-C. Zhou, *J. Am. Chem. Soc.* **2020**, *142*, 12515-12523; d) A. Dhakshinamoorthy, A. M. Asiri, H. Garcia, *Angew. Chem., Int. Ed.* **2016**, *55*, 5414-5445.
- [9] a) H.-X. Zhang, Q.-L. Hong, J. Li, F. Wang, X. Huang, S. Chen, W. Tu, D. Yu, R. Xu, T. Zhou, J. Zhang, *Angew. Chem., Int. Ed.* **2019**, *58*, 11752-11756; b) N. Li, J. Liu, J.-J. Liu, L.-Z. Dong, Z.-F. Xin, Y.-L. Teng, Y.-Q. Lan, *Angew. Chem., Int. Ed.* **2019**, *58*, 5226-5231.
- [10] a) W. Zhou, D.-D. Huang, Y.-P. Wu, J. Zhao, T. Wu, J. Zhang, D.-S. Li, C. Sun, P. Feng, X. Bu, *Angew. Chem., Int. Ed.* **2019**, *58*, 4227-4231; b) H. Dong, X. Zhang, Y. Lu, Y. Yang, Y.-P. Zhang, H.-L. Tang, F.-M. Zhang, Z.-D. Yang, X. Sun, Y. Feng, *Appl. Catal. B: Environ.* **2020**, *276*, 119173-119180.
- [11] D. Li, M. Kassymova, X. Cai, S.-Q. Zang, H.-L. Jiang, *Coord. Chem. Rev.* **2020**, *412*, 213262-213277.
- [12] a) R. Qin, K. Liu, Q. Wu, N. Zheng, *Chem. Rev.* **2020**, *10.1021/acs.chemrev.0c00094*; b) J. Fu, K. Jiang, X. Qiu, J. Yu, M. Liu, *Mater. Today* **2020**, *32*, 222-243; c) J. Duan, Y. Li, Y. Pan, N. Behera, W. Jin, *Coord. Chem. Rev.* **2019**, *395*, 25-45; d) W. Liu, X. Li, C. Wang, H. Pan, W. Liu, K. Wang, Q. Zeng, R. Wang, J. Jiang, *J. Am. Chem. Soc.* **2019**, *141*, 17431-17440.
- [13] a) B. Han, X. Ou, Z. Deng, Y. Song, C. Tian, H. Deng, Y.-J. Xu, Z. Lin, *Angew. Chem., Int. Ed.* **2018**, *57*, 16811-16815; b) G. Lan, Z. Li, S. S. Veroneau, Y.-Y. Zhu, Z. Xu, C. Wang, W. Lin, *J. Am. Chem. Soc.* **2018**, *140*, 12369-12373; c) W. Zhu, C. Zhang, Q. Li, L. Xiong, R. Chen, X. Wan, Z. Wang, W. Chen, Z. Deng, Y. Peng, *Appl. Catal. B: Environ.* **2018**, *238*, 339-345.
- [14] a) J. Huang, Y. Li, R.-K. Huang, C.-T. He, L. Gong, Q. Hu, L. Wang, Y.-T. Xu, X.-Y. Tian, S.-Y. Liu, Z.-M. Ye, F. Wang, D.-D. Zhou, W.-X. Zhang, J.-P. Zhang, *Angew. Chem., Int. Ed.* **2018**, *57*, 4632-4636; b) J. Xiong, L. Wen, F. Jiang, Y. Liu, S. Liang, L. Wu, *J. Mater. Chem. A* **2015**, *3*, 20627-20632.
- [15] E.-X. Chen, M. Qiu, Y.-F. Zhang, Y.-S. Zhu, L.-Y. Liu, Y.-Y. Sun, X. Bu, J. Zhang, Q. Lin, *Adv. Mater.* **2018**, *30*, 1704388.
- [16] a) Y.-S. Kang, Y. Lu, K. Chen, Y. Zhao, P. Wang, W.-Y. Sun, *Coord. Chem. Rev.* **2019**, *378*, 262-280; b) X. Zhao, M. S. Shimazu, X. Chen, X. Bu, P. Feng, *Angew. Chem., Int. Ed.* **2018**, *57*, 6208-6211.
- [17] Y. Wang, X. Jia, H. Yang, Y. Wang, X. Chen, A. N. Hong, J. Li, X. Bu, P. Feng, *Angew. Chem., Int. Ed.* **2020**, DOI: 10.1002/anie.202008696.
- [18] M. Z. Rahman, P. C. Tapping, T. W. Kee, R. Smernik, N. Spooner, J. Moffatt, Y. Tang, K. Davey, S.-Z. Qiao, *Adv. Funct. Mater.* **2017**, *27*, 1702384.
- [19] W. Chen, B. Han, C. Tian, X. Liu, S. Liang, H. Deng, Z. Lin, *Appl. Catal. B: Environ.* **2019**, *244*, 996-1003.
- [20] a) X.-K. Wang, J. Liu, L. Zhang, L.-Z. Dong, S.-L. Li, Y.-H. Kan, D.-S. Li, Y.-Q. Lan, *ACS Catal.* **2019**, *9*, 1726-1732; b) H. Zhang, J. Wei, J. Dong, G. Liu, L. Shi, P. An, G. Zhao, J. Kong, X. Wang, X. Meng, J. Zhang, J. Ye, *Angew. Chem., Int. Ed.* **2016**, *55*, 14310-14314.
- [21] a) D.-C. Liu, H.-H. Huang, J.-W. Wang, L. Jiang, D.-C. Zhong, T.-B. Lu, *ChemCatChem* **2018**, *10*, 3435-3440; b) S. Wang, W. Yao, J. Lin, Z. Ding, X. Wang, *Angew. Chem., Int. Ed.* **2014**, *53*, 1034-1038.
- [22] a) L.-Y. Wu, Y.-F. Mu, X.-X. Guo, W. Zhang, Z.-M. Zhang, M. Zhang, T.-B. Lu, *Angew. Chem., Int. Ed.* **2019**, *58*, 9491-9495; b) L. Buzzetti, G. E. M. Crisenza, P. Melchiorre, *Angew. Chem., Int. Ed.* **2019**, *58*, 3730-3747.
- [23] a) H.-Q. Xu, J. Hu, D. Wang, Z. Li, Q. Zhang, Y. Luo, S.-H. Yu, H.-L. Jiang, *J. Am. Chem. Soc.* **2015**, *137*, 13440-13443; b) Z.-H. Yan, M.-H. Du, J. Liu, S. Jin, C. Wang, G.-L. Zhuang, X.-J. Kong, L.-S. Long, L.-S. Zheng, *Nat. Commun.* **2018**, *9*, 1-9.
- [24] J. Xie, X. Zhao, M. Wu, Q. Li, Y. Wang, J. Yao, *Angew. Chem., Int. Ed.* **2018**, *57*, 9640-9644.

Entry for the Table of Contents



Based on rational structural design and structure-directed morphology control, two new 2D MOFs undergo photochemically-assisted *in-situ* exfoliation forming nanosheets during the visible-light photocatalytic CO₂ reduction with excellent activity and high selectivity.